Processing and Application of Ceramics 18 [2] (2024) 123–129
https://doi.org/10.2298/PAC2402123W

Investigation of Gd, Ca and Nd tri-doped ceria for application in solid oxide fuel cells

Ming Wang, Yifeng Hou, Jihai Cheng*

School of Energy Materials and Chemical Engineering, Hefei University, Hefei, 230022, China

Received 30 December 2023; Received in revised form 22 March 2024; Accepted 10 May 2024

Abstract

Nanosized tri-doped ceria powders with composition $Ce_{0.8}Gd_{0.15}Ca_{0.05-x}Nd_xO_{2-\delta}$ (CGCN, x = 0.0125, 0.025, 0.0375) were obtained by sol-gel methods. The powders were compressed into discs and sintered in air to form perspective solid electrolytes. The obtained samples were characterized by X-ray diffraction (XRD), scanning electron microscopy (SEM) and electrochemical impedance spectroscopy (EIS) methods. XRD and SEM analyses confirm that the samples are densified and have fluorite structure after sintering at 1350 °C. Among all $Ce_{0.8}Gd_{0.15}Ca_{0.05-x}Nd_xO_{2-\delta}$ samples, the sintered $Ce_{0.8}Gd_{0.15}Ca_{0.025}Nd_{0.025}O_{2-\delta}$ electrolyte has the highest conductivity of 2.5×10^{-2} S/cm at 800 °C and the corresponding activation energy is 0.64 eV.

Keywords: *solid oxide fuel cells, electrolyte, doped-CeO_2, structure, electrical conductivity*

I. Introduction

With the rapid development of industry and economy, energy has become the lifeblood of the world's development. The excessive use of fossil fuels causes resource scarcity and environmental pollution, endangering human health and social development. Therefore, the exploration of new energy sources such as renewable energy and green energy has increasingly attracted people's attention [1,2]. Solid oxide fuel cell (SOFC) can directly convert chemical energy into electrical energy, and has an all-solid structure without electrolyte leakage. It is therefore considered to be one of the cleanest and most efficient energy technologies in a wide range of environmentally friendly energy conversion devices [3,4]. At the same time, SOFCs typically operate at higher temperatures (between 400 to 1000 °C), effectively accelerating electrode reaction kinetics and eliminating the need for precious metal catalysts. In addition, SOFCs also have the advantage of fuel flexibility. For this reason, SOFCs are considered one of the most promising fuel cell types.

Most studies on electrolyte materials focus on oxides with cubic fluorite structure, such as stable zirconia, doped bismuth oxide and doped cerium dioxide [5–7]. By doping divalent or trivalent heterovalent cations in fluorite oxides, especially alkaline earth metal oxides or rare earth oxides, charge compensation occurs through the formation of oxygen vacancies, which can significantly improve the ionic conductivity of these materials [8]. It has been found that CeO_2 doped with divalent dopants has less free oxygen vacancies than that doped with trivalent dopants, and dopant-vacancy association increases with the ionic radius of divalent dopant cations [9]. Sun *et al.* [10] found that the rare earth ions doped CeO_2 can form charge-compensated vacancies, and there are many factors that affect the ionic conductivity. Rare earth dopants not only reduce the migration barrier, but also promote the formation of intrinsic vacancies (oxygen vacancies due to thermal excitation). In recent years, researchers have tried to use one or two elements to co-dope samarium doped ceria ($Ce_{0.8}Sm_{0.2}O_{1.9}$, SDC) or gadolinium doped cerium oxide ($Ce_{0.8}Gd_{0.2}O_{1.9}$, GDC) to improve their conductivity or change sintering properties and stability. Two above mentioned electrolytes are considered as the most promising substitutes for YSZ in the intermediate temperature SOFC (IT-SOFC) [11]. Numerous studies have been reported on the co-doping of CeO_2 materials with Ca, Mg, Cu, Sr, La, Y, Er and Sm or Gd [12–17]. The results show that double or triple doping can improve the conductivity of CeO_2 matrix, and the conductivity of this kind of material can reach $1.1–4.2 \times 10^{-2}$ S/cm at 700 °C.

*Corresponding authors: tel: +86 551 62148442,
e-mail: *cjh@hfuu.edu.cn*

Doping can cause lattice strain of CeO_2. In principle, the radius of the doped ions should be close to that of Ce^{4+}, but even so, the doped ions will still affect the lattice. Some studies have calculated the effect of lattice strain on the ionic conductivity of doped CeO_2 [18,19]. The results show that the strain has a great effect on the properties of doped CeO_2. The compressive strain results in lower diffusion coefficient and higher binding energy between the oxygen vacancy and the dopant ions, while the tensile strain results in higher diffusion coefficient and lower binding energy. In addition, the doping can also remove the impurities at the grain boundary of the electrolyte and reduce the grain boundary resistance. SiO_2 impurities may be introduced during ceramic processing, moulding and sintering [20]. These impurities are often accumulated at the grain boundary and cause the grain boundary resistance to increase. The grain boundary resistance can be reduced by adding grain boundary improver. At present, the dopants which can be used to remove impurities at the grain boundary are CaO, SrO, etc. Moure *et al.* [21] increased the grain boundary conductivity of Gd^{3+}-doped CeO_2 by 10-times by adding 2 mol% CaO without affecting the conductivity within the grain.

In this paper, we investigated $Ce_{0.8}Gd_{0.2}O_{1.9}$ composition and added CaO as grain boundary improver to reduce the grain boundary resistance. At the same time, Nd^{3+} was used as the co-dopant to improve the conductivity. The total doping amount in CeO_2 was 20 mol% since the Gd^{3+} content was 15 mol% and the sum of Ca^{2+} and Nd^{3+} contents was 5 mol%. Moreover, the content of Nd was varied (x), thus the content of Ca and Nd maintained a certain ratio. We prepared Ca, Nd and Gd tri-doped CeO_2 ($Ce_{0.8}Gd_{0.15}Ca_{0.05-x}Nd_xO_{2-\delta}$) based electrolyte materials by sol-gel method, powder compaction and sintering. The aim of the present study was to estimate the usability of Ca, Nd and Gd tri-doped doped ceria as a perspective electrolyte for SOFCs. It was expected that the exploration of the high performance electrolyte materials with high oxygen ion conductivity, low polarization resistance and good compatibility with electrode materials will provide new ideas for the development of SOFCs.

II. Experimental

The $Ce_{0.8}Gd_{0.15}Ca_{0.05-x}Nd_xO_{2-\delta}$ (x = 0.0125, 0.025, 0.0375) powders were synthesized by a sol-gel method. The nitrates of $RE(NO_3)_3 \cdot H_2O$ (RE = Ce, Gd, Nd) and $Ca(NO_3)_2 \cdot H_2O$ (analytical grade, Sinopharm Chemical Reagent Co. Ltd.) were used as raw materials. Stoichiometric raw materials were dissolved in deionized water and then citric acid with 1.5 times the molar number of metal ions was added. The pH value of above solution was adjusted to 7–8 with ammonia and stirred at 60 °C till a homogeneous sol formed. After heating the sol at 80 °C for about 1 h, a white gel was obtained. The gel was dried for 24 h in an oven at 120 °C and then calcined at 750 °C to get the precursor powders. The powders were evenly mixed with a small amount of PVA (about 3–5% by mass of the powder), and then pressed into discs with size of ⌀12 × 1 mm under 200 MPa, and finally sintered at different temperatures (1200–1400 °C) in air for 2 h to form electrolyte ceramics.

The structure and phase composition of the samples were characterized using X-ray diffraction (XRD). Archimedes method was used to determine the density of the sintered body. The microstructure of the specimens was observed by scanning electron microscopy (SEM). By using electrochemical impedance spectroscopy (EIS), the conductivity of the specimens was measured between 500 and 800 °C with an interval of 50 °C in air. Before the impedance test, Ag electrode was formed by painting silver paste on both sides of the discs and fired at 700 °C for 0.5 h. The electrical conductivity of the samples was calculated using the formula of $\sigma = L/(R \cdot S)$, where L was the thickness and S was the electrode area of the samples, while the resistance R was measured by fitting the impedance spectrum with ZSimpWin software. Activation energies (E_a) were calculated by fitting the conductivity data to the Arrhenius equation:

$$\sigma \cdot T = A \cdot \exp\left(-\frac{E_a}{k \cdot T}\right) \tag{1}$$

where σ, A, E_a, k and T were conductivity, pre-exponential factor, activation energy, Boltzmann constant and temperature, respectively.

III. Results and discussion

3.1. Structure analyses

X-ray diffraction patterns of the tri-doped samples sintered at 1350 °C are presented in Fig. 1. From XRD results, it can be observed that the single phase of ceria with a cubic fluorite structure which matched well with

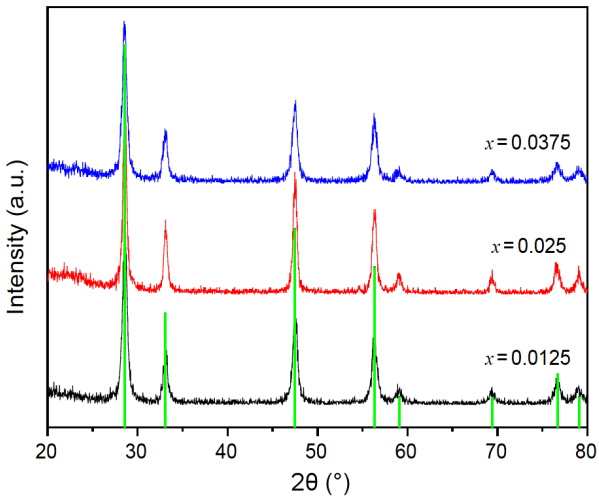

Figure 1. XRD patterns of $Ce_{0.8}Gd_{0.15}Ca_{0.05-x}Nd_xO_{2-\delta}$ samples sintered at 1350 °C with different doping amounts (green lines represent the standard diffraction peak of CeO_2, JCPDS 42-1121)

Table 1. Lattice constant (a), relative density (ρ_r), conductivity (σ) and activation energy (E_a) of $Ce_{0.8}Gd_{0.15}Ca_{0.05-x}Nd_xO_{2-\delta}$ samples sintered at 1350 °C

x	a [nm]	ρ_r [%]	σ [S/cm]*	E_a [eV]*
0.0125	0.5419	95.37	0.022	0.72
0.025	0.5421	95.21	0.025	0.64
0.0375	0.5426	95.86	0.019	0.69

* σ and E_a were calculated from the impedance spectra of the samples tested at 800 °C

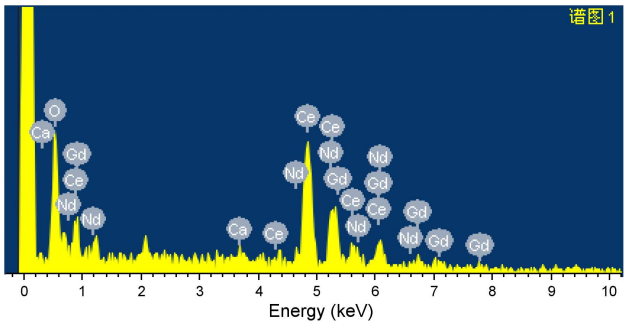

Figure 2. EDX spectrum of $Ce_{0.8}Gd_{0.15}Ca_{0.025}Nd_{0.025}O_{2-\delta}$ sample sintered at 1350 °C

JCPDS42-1121 (CeO_2) was formed, and there was no diffraction peak of any impurity phase, such as: Gd_2O_3, Nd_2O_3 and CaO. This means that the CeO_2 has been fully stabilized by Gd_2O_3, Nd_2O_3 and CaO. Thus, the sintered samples as solid ionic conductors retained the same structure as CeO_2, which confirmed that Ce^{4+} ions in the crystal lattice of the CeO_2 were replaced successfully by dopant ions.

Since the lattice constants are considered useful tools to predict electrical conductivity behaviour, the XRD patterns were fitted using Jade software and the lattice parameter of the tri-doped ceria powders was calculated (Table 1). Results showed that the determined lattice parameter values for the tri-doped CeO_2 and pure CeO_2 agreed quite well. In other words, the main purpose of doping ceria with lower valent cations was to introduce oxygen vacancies into the CeO_2 crystal lattice to improve the ionic conductivity, while retaining the lattice parameter similar to the one of pure CeO_2 [22].

In order to analyse the composition of the fluorite-type tri-doped CeO_2 phases, the EDX analysis was performed (Fig. 2). It confirmed that 1.19 at.% Ca and 1.15 at.% Nd were incorporated in the fluorite CeO_2 phases. Thus, the obtained doped-CeO_2 is referred to as $Ce_{0.8}Gd_{0.15}Ca_{0.05-x}Nd_xO_{2-\delta}$ (CGCN). SEM mapping of the $Ce_{0.8}Gd_{0.15}Ca_{0.025}Nd_{0.025}O_{2-\delta}$ sample sintered at 1350 °C is shown in Fig. 3. Separate regions rich in Ce, Gd, Ca and Nd, corresponding to the CeO_2 phases, were observed.

3.2. Microstructure and density

Density is very important characteristic of electrolyte materials and it is closely related to ionic conduction and mechanical properties. Lower density means that there are many pores at the grain boundary, which will inevitably affect the conductivity of electrolyte materials. The actual density of the sintered ceramic discs was measured by the Archimedes drainage method and used for calculation of relative density. The lattice constant of the sintered body was obtained from the XRD results and used to calculate the theoretical density. Figure 4 shows the relative density and linear contraction rate of the $Ce_{0.8}Gd_{0.15}Ca_{0.025}Nd_{0.025}O_{2-\delta}$ sintered sample as a function of temperature. As it can be seen from Fig. 4, the relative density of the $Ce_{0.8}Gd_{0.15}Ca_{0.025}Nd_{0.025}O_{2-\delta}$ sintered at 1350 °C is less than 95 %TD, while the linear shrinkage is less than 10%. When the $Ce_{0.8}Gd_{0.15}Ca_{0.025}Nd_{0.025}O_{2-\delta}$ sample is sintered at 1350 °C, the relative density increases substantially to 95 %TD and the linear shrinkage reaches 10%. The linear shrinkage did not increase signifi-

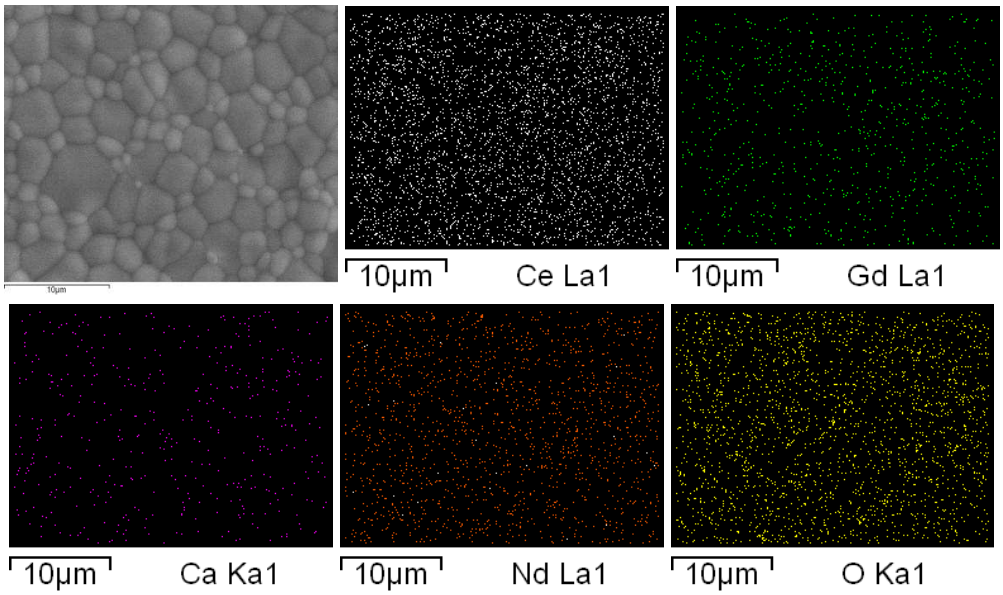

Figure 3. SEM mapping of the $Ce_{0.8}Gd_{0.15}Ca_{0.025}Nd_{0.025}O_{2-\delta}$ sample sintered at 1350 °C

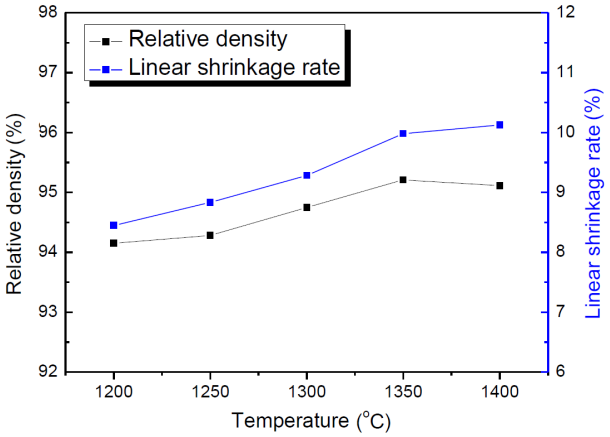

Figure 4. Relative density and linear shrinkage rate of $Ce_{0.8}Gd_{0.15}Ca_{0.025}Nd_{0.025}O_{2-\delta}$ sample as a function of sintering temperature

cantly with the increase of the sintering temperature to 1400 °C. It can also been seen that the relative density increases with the increase of temperature at first, and decreases afterwards. Thus, it reaches a maximum value when the sintering temperature is about 1350 °C. It may be caused by the effect of high temperature on grain growth. When the sintering temperature is too high, the speed of grain growth increases and abnormal growth occurs, which makes the pores in the sample difficult to be expelled, thus the density decreases. Therefore, 1350 °C is selected as the optimal sintering temperature in this study.

SEM images of the $Ce_{0.8}Gd_{0.15}Ca_{0.025}Nd_{0.025}O_{2-\delta}$ sample sintered at different temperatures are shown in Fig. 5. As it can be seen from Fig. 5a, the grains are rounded, the grain boundaries are not obvious and the pores are large in the sample sintered at 1200 °C. At higher sintering temperature (Fig. 5b), grain boundaries are starting to be visible, but there are still a small number of pores. SEM image of the sample sintered at 1350 °C (Fig. 5c) confirms that the grains grow, the grain boundaries are obvious and there are almost no pores in the sample indicating the formation of a dense structure. The excessive growth of the grains and inconspicuous grain boundaries are characteristics of the sample sintered at 1400 °C (Fig. 5d). The high sintering temperature may be the reason for grain boundary sliding.

3.3. Electrical properties

It is well known that electrochemical impedance spectroscopy (EIS) is a common method for studying the electrical properties of fast ion conductors [23]. Besides the total ionic conductivity value, it also provides useful information about the contribution of the grains, grain boundaries and the electrode-electrolyte interface to the total ionic conductivity.

The Nyquist's plots of the sintered $Ce_{0.8}Gd_{0.15}Ca_{0.025}Nd_{0.025}O_{2-\delta}$ samples tested between 500–800 °C with the increments of 50 °C are presented in Fig. 6. It can be seen that the impedance spectrum of the sample tested at 800 °C consists of a complete semicircle and an incomplete semicircle. In general, an impedance spectrum consists of three semicircles corresponding to the grain conduction, grain boundary conduction and electrode-electrolyte interface conduction, respectively. But at higher temperatures (600–800 °C), the correlation with grain impedance is much smaller than the electrode process, so the semicircle at high frequency disappears [24–26].

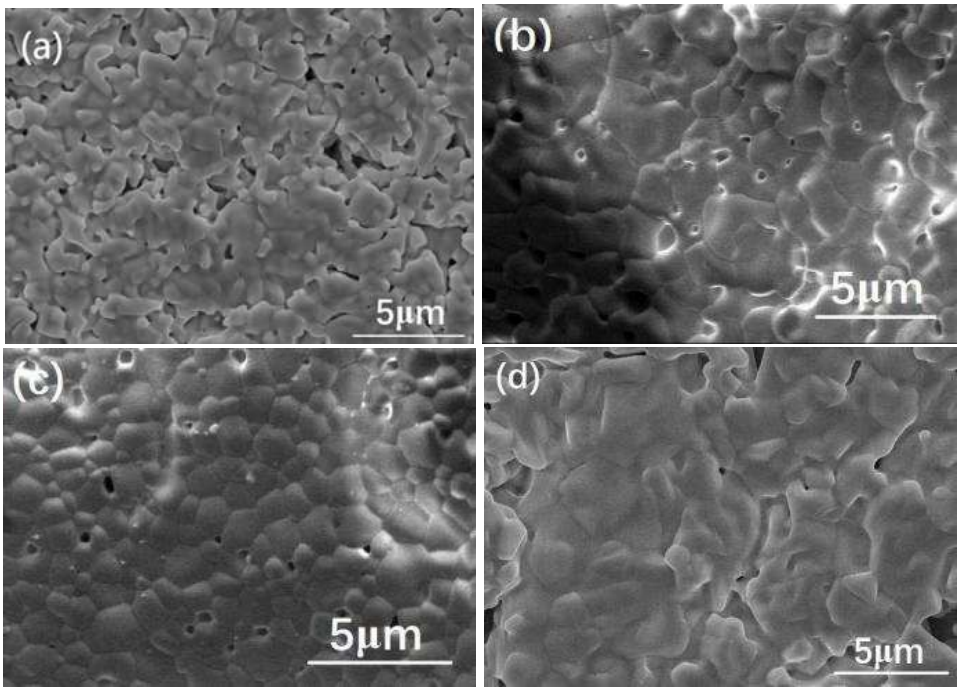

Figure 5. SEM images of $Ce_{0.8}Gd_{0.15}Ca_{0.025}Nd_{0.025}O_{2-\delta}$ electrolyte ceramics sintered at: a) 1200 °C, b) 1300 °C, c) 1350 °C and d) 1400 °C

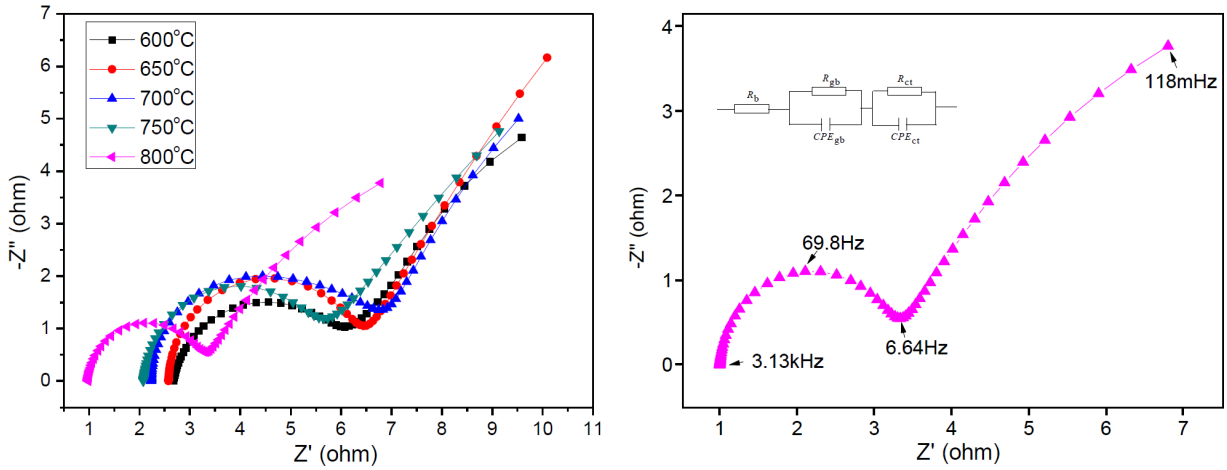

Figure 6. The Nyquist's plots of $Ce_{0.8}Gd_{0.15}Ca_{0.025}Nd_{0.025}O_{2-\delta}$ sample

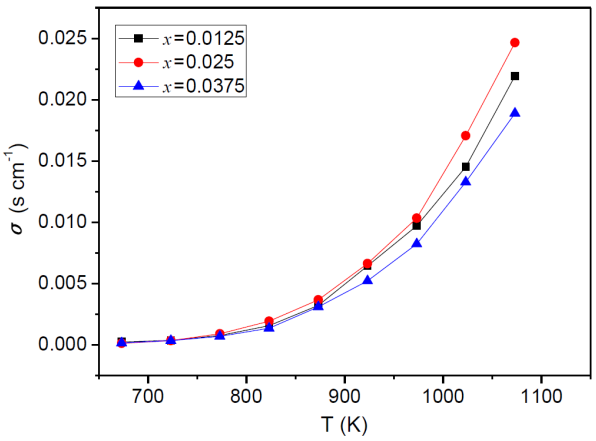

Figure 7. Conductivity of $Ce_{0.8}Gd_{0.15}Ca_{0.05-x}Nd_xO_{2-\delta}$ sintered sample as a function of temperature

The observed two semicircles could be attributed to bulk and grain boundary responses, respectively. The values R_b and R_{gb} were estimated from the cross sections of obtained semicircles with the Re(Z) axis [27,28]. The impedance spectra data were fitted with the ZSimpWin software to determine bulk resistance (R_b), grain-boundary resistance (R_{gb}), and the total resistance (R_t) should be defined as $R_t = R_b + R_{gb}$. While the total conductivity (σ) of samples is defined as $\sigma = L/(R \cdot S)$, where L, R and S are the thickness of sintered disc, total resistance and electrode area, respectively. With the increase of the testing temperature, the arc at the high frequency end gradually disappears and the radius of the semicircles gradually decreases. It indicates that the bulk and grain boundary semicircles are closely related to the test temperature, and the increase of temperature will lead to the decrease in bulk and grain boundary resistances.

Figure 7 shows the conductivity of the $Ce_{0.8}Gd_{0.15}Ca_{0.05-x}Nd_xO_{2-\delta}$ sintered samples as a function of temperature. As the Nd doping increases, the electrical conductivity decreases at first, then increases to a maximum value, and then decreases again. Among all the samples, the conductivity reaches its maximum at $x = 0.025$ and it can reach 0.025 S/cm at 800 °C. The main reason for the increase of conductivity is that when Ca and Nd are doped in GDC, part of Gd^{3+}, Ca^{2+} and Nd^{3+} take the place of Ce^{4+}. In order to keep the electrical neutrality of the material, a certain amount of oxygen vacancies is created in the crystal to increase the conductivity of the sample. Accordingly, the conductivity increases with the increase of oxygen vacancy. With the increase of doping amount, the formation of defect associations depletes part of the oxygen vacancies and results in the decrease of conductivity. Because of the above two reasons, gadolinium doped cerium oxide (GDC) exhibits superior conductivity at a certain ratio of Ca/Nd ($x = 0.025$) [8,29].

A recent literature review containing results of total ionic conductivity values for different electrolyte materials based on doped ceria is presented in Table 2. The conductivity of the samples in present work is close to or superior to other similar electrolyte materials. Thus,

Table 2. Total conductivity of doped CeO_2 electrolytes

Electrolyte material	Total ionic conductivity [S/cm]	Temperature [°C]	Reference
$Ce_{0.8}Gd_{0.15}Ca_{0.025}Nd_{0.025}O_{2-\delta}$	0.025	800	Present work
$Ce_{0.85}La_{0.10}Sm_{0.05}O_2$	0.075	750	[30]
10 mol% Gd-doped CeO_2	5.71×10^{-4}	400	[31]
$Dy_{0.1}Ce_{0.90}O_{1.95}$	$1 \times 10^{-1.91}$	650	[32]
Co-$Ce_{0.6}La_{0.4}O_{2-\delta}$	8.68×10^{-3}	700	[33]
$Ce_{0.8}Y_{0.15}Ca_{0.05}O_{2-\delta}$	0.1	800	[34]

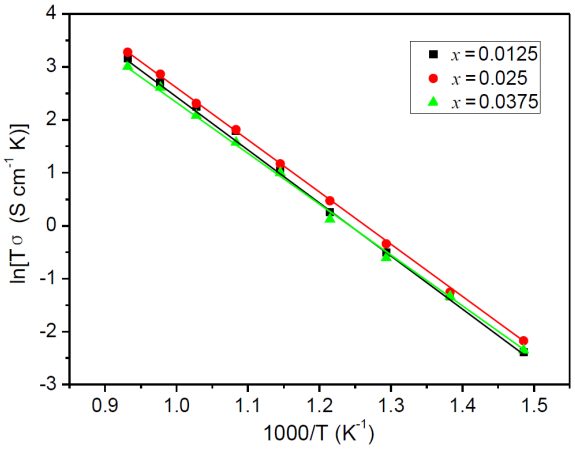

Figure 8. The Arrhenius plots of the conductivities of $Ce_{0.8}Gd_{0.15}Ca_{0.05-x}Nd_xO_{2-\delta}$ samples

this electrolyte has the potential to be used as high-temperature solid electrolyte materials in the solid oxide fuel cell.

Figure 8 shows the Arrhenius curves of electrical conductivity at 400–800 °C of the $Ce_{0.8}Gd_{0.15}Ca_{0.05-x}Nd_xO_{2-\delta}$ electrolyte ceramics sintered at 1350 °C in air at 400–800 °C. The change trend of the activation energy is similar to that of the conductivity, that is, with the increase of Nd doping amount, the activation energy decreases at first and then increases. When x = 0.0125, 0.025 and 0.0375, the average activation energy of the $Ce_{0.8}Gd_{0.15}Ca_{0.05-x}Nd_xO_{2-\delta}$ sintered samples were 0.72, 0.64 and 0.69 eV, respectively. The reason is that when the doping amount of Nd is low, the oxygen vacancy in the lattice becomes disordered to some extent, and the mobility of oxygen ions is enhanced. However, when the doping amount increases, the excess Nd_2O_3 can be released at the grain boundary, which hinders the movement of oxygen ions and thus increases the migration energy of oxygen ions [35,36]. This result is consistent with the change trend of electrical conductivity.

IV. Conclusions

The $Ce_{0.8}Gd_{0.15}Ca_{0.05-x}Nd_xO_{2-\delta}$ (x = 0.0125, 0.025, 0.0375) electrolyte powders were prepared by a sol-gel method. The prepared powders had high sintering activity and they were easily densified to the required density higher than 95 %TD for electrolyte materials, XRD results show that the samples sintered at 1350 °C had single phase fluorite structure without any impurity phase. The conductivity of the $Ce_{0.8}Gd_{0.15}Ca_{0.05-x}Nd_xO_{2-\delta}$ samples is significantly affected by addition of appropriate amount of Ca^{2+} and Nd^{3+} ions. When the Nd^{3+} doping content is 2.5 mol%, the conductivity reaches a maximum value of 0.025 S/cm at 800 °C. Therefore, when co-doped with an appropriate Ca/Nd ratio, the electrical conductivity of the $Ce_{0.8}Gd_{0.15}Ca_{0.05-x}Nd_xO_{2-\delta}$ will be effectively increased and it can be used as a potential electrolyte for solid oxide fuel cells (SOFCs).

Acknowledgements: This project is supported by the Nature Science Foundation of Anhui Province of China under contact No. 2108085ME152.

References

1. N. David, S. Gunn, J.A. Purtona, "Adaptive kinetic Monte Carlo simulation of solid oxide fuel cell components", *J. Mater. Chem. A,* **2** (2014) 13407–13414.
2. C.M. Xu, S.Y. Zhen, R.Z. Ren, H.S. Chen, W.L. Song, Z.H. Wang, W. Sun, K.N. Sun, "Cu-doped $Sr_2Fe_{1.5}Mo_{0.5}O_{6-\delta}$ as a highly active cathode for solid oxide electrolytic cells", *Chem. Commun.,* **55** (2019) 8009–8012.
3. Y.P. Xia, Z.L. Jin, H.Q. Wang, Z. Gong, H.L. Lv, R.R. Peng, W. Liu, L. Bi, "A novel cobalt-free cathode with triple-conduction for proton-conducting solid oxide fuel cells with unprecedented performance", *J. Mater. Chem. A,* **7** (2019) 16136–16148.
4. C. Zhao, T. Zhang, Y. He, L.W. Qu, Q.J. Zhou, "Preparation and performance of $Sr_3Fe_{2-x}Ni_xO_{7-\delta}$ (x = 0, 0.1, 0.2, 0.3) cathode for Intermediate-Temperature Solid Oxide Fuel Cells", *Chinese J. Inorg. Chem.,* **35** (2019) 1027–1033.
5. S. Dwivedi, "Solid oxide fuel cell: Materials for anode, cathode and electrolyte", *Int. J. Hydrogen Energ.,* **45** (2020) 23988–24013.
6. W.X. Qian, H. Liang, X.H. Zhu, J.H. Cheng, "The effect of Y, Er co-doped on the sintering and electrical properties of $Mo_{0.05}Bi_{1.95}O_3$ electrolyte materials for solid oxide fuel cells", *Funct. Mater. Lett.,* **16** (2023) 2350017.
7. D.H. Lee, K.S. Cha, Y.S. Lee, K.S. Kang, C.S. Park, Y.H. Kim, "Effects of CeO_2 additive on redox characteristics of Fe-based mixed oxide mediums for storage and production of hydrogen", *Int. J. Hydrogen Energ.,* **34** (2009) 1417–1422.
8. D. Zhou, Y. Xia, J. Zhu, W. Guo, J. Meng, "Preparation and electrical properties of new oxide ion conductors $Ce_{6-x}Gd_xMoO_{15-\delta}$ ($0.0 \leq x \leq 1.8$)", *J. Am. Ceram. Soc.,* **92** (2009) 1042–1046.
9. S. Anirban, P.T. Das, A. Dutta, "Effect of divalent cation addition on structure, conductivity and grain boundary properties in La doped ceria oxygen ion conductors", *Ceram. Int.*, **45** (2019) 5751–5760.
10. Q. Sun, Z.M. Fu, Z.X. Yang, "Effects of rare-earth doping on the ionic conduction of CeO_2 in solid oxide fuel cells", *Ceram. Int.*, **44** (2018) 3707–3711.
11. M. Mogensen, N.M. Sammes, "Physical, chemical and electrochemical properties of pure and doped ceria", *Solid State Ionics*, **129** (2000) 63–94.
12. J.H. Cheng, C.A. Tian, J. Yang, "Effects of Mg^{2+} addition on structure and electrical properties of gadolinium doped ceria electrolyte ceramics", *Process. Appl. Ceram.,* **13** (2019) 182–188.
13. M. Anwar, M.A. Sa, N.A. Baharuddin, N.F. Raduwan, A. Muchtar, M.R. Somalu, "Structural, optical and electrical properties of $Ce_{0.8}Sm_{0.2-x}Er_xO_{2-\delta}$ (x = 0–0.2) co-doped ceria electrolytes", *Ceram. Int.*, **44** (2018) 13639–13648.
14. M. Anwar, M.A. Sa, A. Muchtar, M.R. Somalu, "Influence of strontium co-doping on the structural, optical, and electrical properties of erbium-doped ceria electrolyte for intermediate temperature solid oxide fuel cells", *Ceram. Int.*, **45** (2019) 5627–5636.

15. Z.L. Zhan, T.L. Wen, H.Y. Tu, Z.Y. Lu, "AC Impedance investigation of samarium-doped ceria", *J. Electrochem. Soc.,* **148** (2001) A427–A432.
16. A. Arabaci, V. Sariboga, M. Öksuzomer, "Er and Gd co-doped ceria-based electrolyte materials for IT-SOFCs prepared by the Cellulose-templating method", *Metall. Mater. Trans. A*, **45** (2014) 5259–5269.
17. M. Singh, A.K. Singh, "Studies on structural, morphological, and electrical properties of Ga^{3+} and Cu^{2+} co-doped ceria ceramics as solid electrolyte for IT-SOFCs", *Int. J. Hydrogen Energ.,* **45** (2020) 24014–24025.
18. M.J.D. Rushton, A. Chroneos, S.J. Skinner, J.A. Kilner, R.W. Grimes, "Effect of strain on the oxygen diffusion in yttria and gadolinia co-doped ceria", *Solid State Ionics*, **230** (2013) 37–42.
19. K. Ahn, Y.C. Chung, K.J. Yoon, J.W. Son, B.K. Kim, H.W. Lee, J.H. Lee, "Lattice-strain effect on oxygen vacancy formation in gadolinium-doped ceria", *J. Electroceram.*, **32** (2014) 72–77.
20. B.C.H. Steele, "Appraisal of $Ce_{1-y}Gd_yO_{2-y/2}$ electrolytes for IT-SOFC operation at 500 °C", *Solid State Ionics*, **129** (2000) 95–110.
21. A. Moure, J. Tartaj, C. Moure, "Synthesis, sintering and electrical properties of gadolinia-calcia-doped ceria", *Mater. Lett.*, **65** (2011) 89–91.
22. M. Stojmenović, S. Bošković, S. Zec, B. Babić, B. Matović, D. Bučevac, Z. Dohčević-Mitrović, F. Aldinger, "Characterization of nanometric multidoped ceria powders", *J. Alloys Compd.*, **507** (2010) 279–285.
23. E. Drożdż, J. Wyrwa, K. Schneider, M. Rękas, "Electrical properties of silica-doped 3 mol% yttria-stabilized tetragonal zirconia", *J. Mater. Sci.,* **52** (2016) 674–685.
24. T.H. Hsieh, D.T. Ray, Y.P. Fu, "Co-precipitation synthesis and AC conductivity behavior of gadolinium-doped ceria", *Ceram. Int.,* **39** (2013) 7967–7973.
25. K.C. Anjaneya, G.P. Nayaka, J. Manjanna, G. Govindaraj, K.N. Ganesha, "Preparation and characterization of $Ce_{1-x}Gd_xO_{2-\delta}$ (x = 0.1-0.3) as solid electrolyte for intermediate temperature SOFC", *J. Alloys Compd.,* **578** (2013) 53–59.
26. N.K. Singh, P. Singh, M.K. Singh, D. Kumar, O. Parkash, "Auto-combustion synthesis and properties of $Ce_{0.85}Gd_{0.15}O_{1.925}$ for intermediate temperature solid oxide fuel cells electrolyte", *Solid State Ionics,* **192** (2011) 431–434.
27. M. Stojmenović, N. Nišić, M. Žunić, F. Basoli, J. Gulicovki, I. Ristović, M. Kragović, "Development of a new system of solid ionic conductors based on multi-doped ceria for application in IT-SOFCs", *Process. Appl. Ceram.,* **16** (2022) 391–401.
28. M. Stojmenović, M. Žunić, J. Gulicovski, V. Dodevski, M. Prekajski, A. Radulović, S. Mentus, "Structural, morphological and electrical properties of $Ce_{1-x}Ru_xO_{2-\delta}$ (x = 0.005-0.02) solid solutions", *Ceram. Int.,* **42** (2016) 14011–14020.
29. B. Ji, C. Tian, C. Wang, T. Wu, J. Xie, M. Li, "Preparation and characterization of $Ce_{0.8}Y_{0.2-x}Cu_xO_{2-\delta}$ as electrolyte for intermediate temperature solid oxide fuel cells", *J. Power Sources,* **278** (2015) 420–429.
30. R. Kırkgeçit, H.O. Torun, F.K. Dokan, E. Oztürk, "Optical and electrical conductivity properties of rare earth elements (Sm, Y, La, Er) co-doped CeO_2", *J. Rare Earths*, **40** (2022) 1619–1627.
31. S.S.B. Che Abdullah, T. Teranishi, H. Hayashi, A. Kishimoto, "Enhanced electrical conductivity of doped CeO_2 under millimeter-wave irradiation heating", *Mater. Design*, **115** (2017) 231–237.
32. D.E. Puente-Martínez, J.A. Díaz-Guillen, S.M. Montemayor, J.C. Díaz-Guillen, O. Burciaga-Díaz, M.E. Bazaldúa-Medellín, M.R. Díaz-Guillen, A.F. Fuentes, "High ionic conductivity in CeO_2 SOFC solid electrolytes; Effect of Dy doping on their electrical properties", *Int. J. Hydrogen Energ.*, **45** (2020) 14062–14070.
33. J.-E. Hong, S. Ida, T. Ishihara, "Effects of transition metal addition on sintering and electrical conductivity of La-doped CeO_2 as buffer layer for doped $LaGaO_3$ electrolyte film", *Solid State Ionics*, **262** (2014) 374–377.
34. J. Kang, W. Feng, D. Guo, K. Chen, S. Gao, J. Jiang, C. Lu, B. Niu, B. Wang, "Performance optimization of Ca and Y co-doped CeO_2-based electrolyte for intermediate-temperature solid oxide fuel cells", *J. Alloys Compd.*, **913** (2022) 165317.
35. L. Zhang, F. Liu, K. Brinkman, K.L. Reifsnider, A.V. Virkar, "A study of gadolinia-doped ceria electrolyte by electrochemical impedance spectroscopy", *J. Power Sources*, **247** (2014) 947–960.
36. M. Yashima, "Invited Review: Some recent developments in the atomic-scale characterization of structural and transport properties of ceria-based catalysts and ionic conductors", *Catal. Today,* **253** (2015) 3–19.